11.3.1 Circuit-breaker operation

Physical phenomena appearing during this type of operation may be the same as for the disconnector switch operation but the stress is usually less severe. One particular case is circuit-breaker re-ignition when switching small inductive loads (see IEC 61233).

11.3.2 Internal faults

This is not usually a critical aspect, except for external overvoltages (see 11.3.5).

11.3.3 Earthing switch operation

This is the same mechanism as for internal fault but the stress is less severe.

11.3.4 Internal transients

Internal transients are transients between inner conductors and the encapsulation. The propagation of VFFO throughout GIS can be analysed by representing GIS sections as low-loss distributed parameter transmission lines. The internal damping of the transients influencing the highest frequency components is determined by the spark resistance. Skin effects due to the aluminium enclosure can be neglected. The main portion of the damping of the very-fast-front transients occurs by out-coupling at the transition to the overhead line. The trapped charge remaining on the load side of the disconnector has a strong influence on the level of VFFO. For a normal disconnector, the maximum trapped charge reaches 0,5 p.u. and results in overvoltages in the range of 1,7 p.u. and reach 2,0 p.u. for specific cases.

11.3.5 External transients

The mechanism that generates the external transients from the internal transients can be analysed by considering GIS–air interface to be a connection of three transmission lines as shown in Figure 22. GIS internal transients arriving at the GIS-air interface are then partly transmitted to overhead lines, partly transmitted to enclosure and also partly reflected in the GIS.

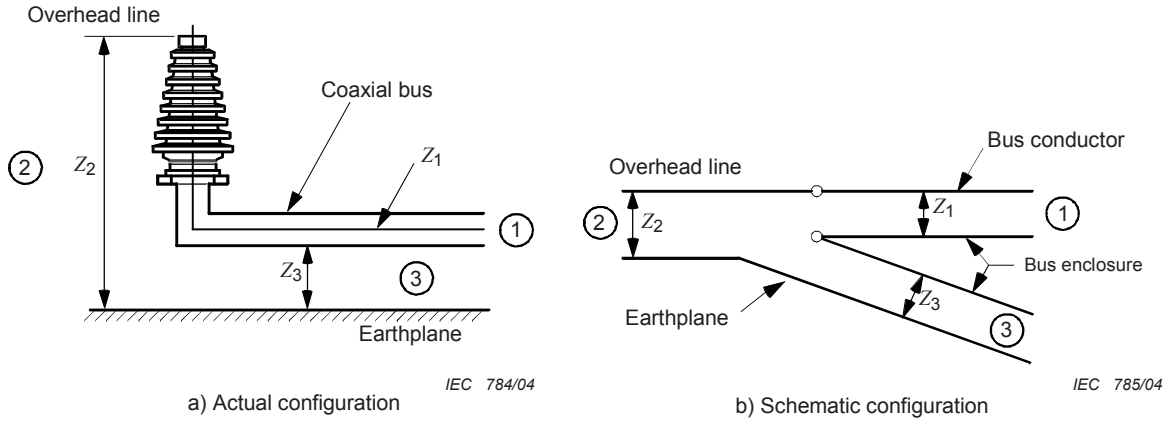

Figure 22 – At the GIS-air interface: coupling between enclosure and earth (Z_3), between overhead line and earth (Z_2) and between bus conductor and enclosure (Z_1) [33]

11.3.5.1 Transient enclosure voltages (TEV)

Transient enclosure voltages are short-duration, high-voltage transients which appear on the enclosure of the GIS through the coupling of internal transients to enclosure at enclosure discontinuities. The usual location for these voltages is the transition GIS-overhead line at an air bushing, such as visual inspection ports, insulated spacers for CTs or insulated flanges at GIS and GIS/cable interfaces. In general, TEV waveforms have at least two components which are damped quickly: the first one has a short initial rise time and is followed by high-frequency oscillations (range of frequency 5 MHz to 10 MHz); the second component is of lower frequency, hundreds of kHz and is often associated with the discharge of capacitive devices to the earthing system. TEV generally persist for a few microseconds. Their magnitude is in the range of 0,1 p.u.to 0,3 p.u.

11.3.5.2 Transients on overhead connections

A portion of the travelling wave incident at a gas-air transition is coupled onto the overhead connections and propagates to other components. In general, it has two different characteristics:

– a fast-front portion having a rise time in the range of 20 ns;

– an overall waveshape having a typical very significant oscillation of frequency in the order of 10 MHz.

11.4 Guideline to perform studies

The main concern from the point of view of insulation co-ordination is related to internal transients. External transients deal with electromagnetic compatibility aspects (transient induction on auxiliary conductors and personnel health and safety). For modern GIS, the main concern is to assess the VFFO occurring when an internal discharge takes place, mainly a disconnector operation.

To perform studies, the system considered is represented using for each component the modelling specified in 7.7.1. The part of the system to be represented in detail is limited to the GIS.

12 Test cases

12.1 General

The aim of this clause is to show how the methodology presented previously can be applied in practical studies. In order to do so, one test case is presented for each type of study.

Supplementary test cases can be found in the annexes .

12.2 Case 1: TOV on a large transmission system including long lines

This section summarizes results of a test case of TOV on a large 735 kV system including long transmission lines. As suggested in 8.3.4, the test case has been performed in two steps:

- Step 1: A stability programme is used to detect the system configurations and events which may lead to severe TOV.
- Step 2: Electromagnetic transient simulations are performed to assess more accurately the level of overvoltages which may appear on the system. Dynamic source models have been used for TOV simulations taking into account the system dynamic behaviour during severe electro-mechanical disturbances that were observed in step 1.

12.2.1 Description of the test-case system

The test-case system, as illustrated in Figure 23, is a long radial system. The three main generating centres, No. 1 (8 100 MW), No. 2 (5 600 MW) and No. 3 (15 600 MW), are far away from the load centre. The length of the two major transmission corridors running from the Nos. 2 and 3 to the load centre is approximately 1 000 km and that from No. 1 to the load centre is about 400 km. The following equipment has been used for reactive power compensation:

- Switched shunt reactors (number of 165/330 MVAr units totalling 25 000 MVAr);
- Synchronous compensators (9×250 MVA);
- Static VAr system (SVS) (11×300 MVAr);
- Series capacitors (32 banks adding up to 11 200 MVAr).

Furthermore, three system-wide automatic switching schemes have also been implemented in this transmission network:

- a shunt reactor automatic switching system called MAIS [40];
- an automatic generation rejection and remote load shedding scheme called RPTC [41];
- an automatic system, namely SPSR, using switched metal-oxide surge arresters (SMOSA) [39], [55].

12.2.2 Step 1: Detection of the system configuration and events leading to severe TOV using a stability programme

System stability study shows that, in case of misoperation of the RPTC, this transmission system could be unstable following a three-phase fault at CHM7 with the loss of three lines: two lines CHM-JCA7 and one line CHM7-SAG7. These disturbances would lead to out-of-phase conditions on the three lines connecting LVD7 to the load centre. Subsequently, the simultaneous tripping of these last three lines by their distance-relay based protections makes the system full-load rejection (or separation). Following a system separation, severe TOV due to Ferranti effects appear on long unloaded lines which are still connected to generating centres. This system separation scenario has been simulated using a stability programme by the following switching sequence:

- At t = 0, the system is under steady-state peak-load flow condition.
- At t = 6 cycles, a three-phase fault at CHM7 is initiated.
- At t = 12 cycles, the three-phase fault at CHM7 is cleared simultaneously with the trip-out of the three lines CHM7-JCA7 and CHM7-SAG7.
- At t = 27 cycles, the total generation of 4 400 MW at TIL7 is successfully rejected by the actions of the RPTC. However, the remote load shedding function is not active due to misoperation of the RPTC.
- At t = 55 cycles, the three lines connecting LVD7 to the load centre are tripped by actions of their distance-relay-based protections under out-of-phase conditions making the system separation.

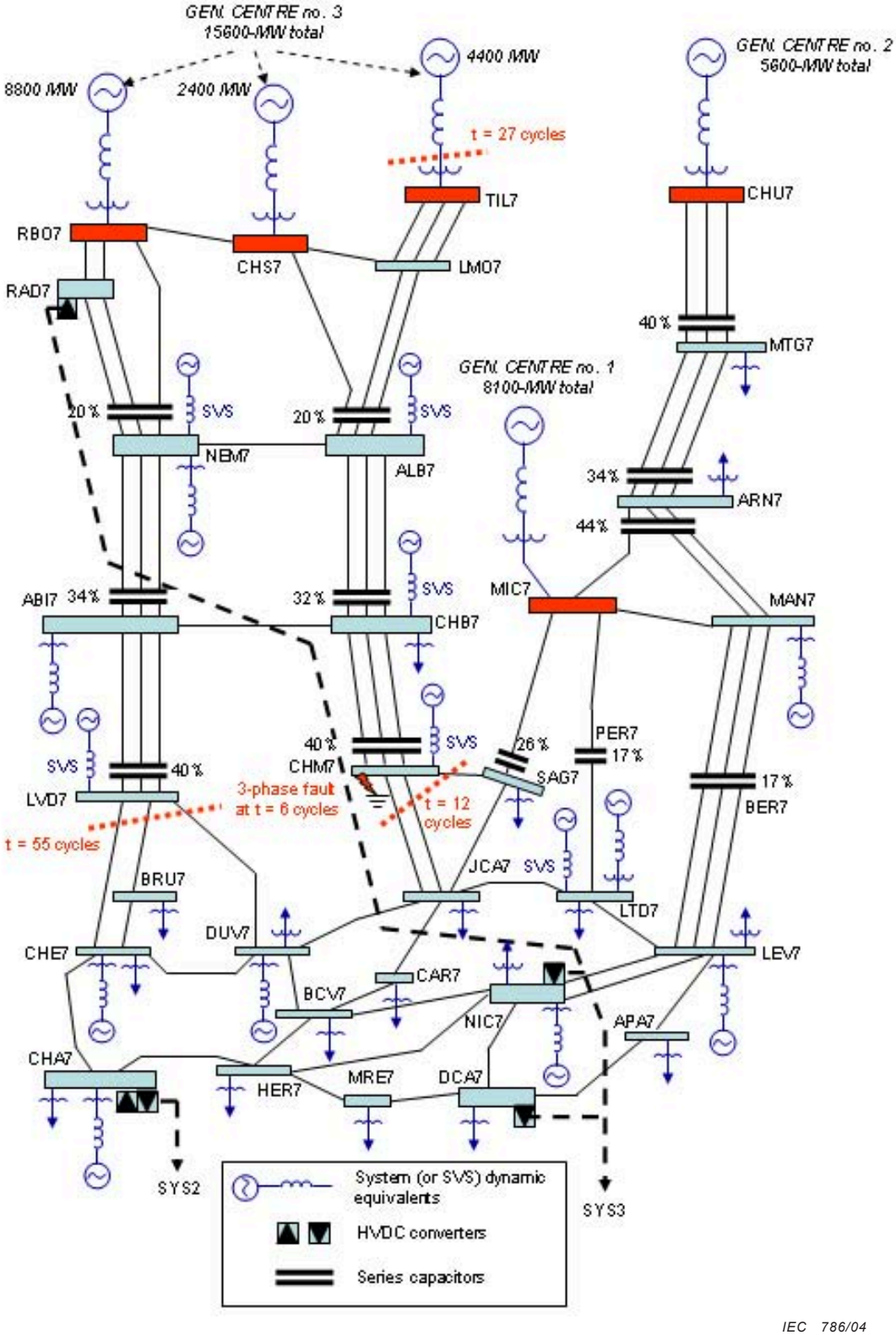

Figure 23 – Single-line diagram of the test-case system

The results of the stability programme are illustrated in Figures 24 and 25. Following three-phase fault clearing and loss of the three lines CHM7-JCA7 and CHM7-SAG7, the rates of rise in frequency at the various generating centres are not the same. Out-of-phase conditions between No. 3 and Nos. 1 and 2 are reached at t = 55 cycles (0,9166 s) when the difference in frequency of these generating centres is approximately equal to 1,0 Hz or 0,016 p.u., as illustrated in Figure 25. At the same instant, the voltages at LVD7 and CHE7 reach their minimum before the system separation takes place (Figure 24). Following the system separation, very high TOV occur on long unloaded and slightly compensated lines that are left connected to generating centre No. 3. As a result, the prospective TOV of 2,5-2,7 p.u. were observed at LVD7 and CHM7. These prospective TOV are much more severe than those occurring on the sound phases during single phase-to-earth faults. Although voltage regulators in generating centre No. 3 tend to reduce the magnitude of prospective TOV over a time period of 30 cycles, their effects are not sufficient to bring TOV down to a safer level for system equipment (Figure 24). It should be mentioned that the results of the stability programme do not include the non-linear effects of transformer saturation and metal-oxide surge arresters. These effects limit the expected TOV on the real system. Therefore, detailed electromagnetic transient simulation including system dynamic behaviour, transformer saturation and metal-oxide surge arresters is needed in order to obtain more realistic TOV.

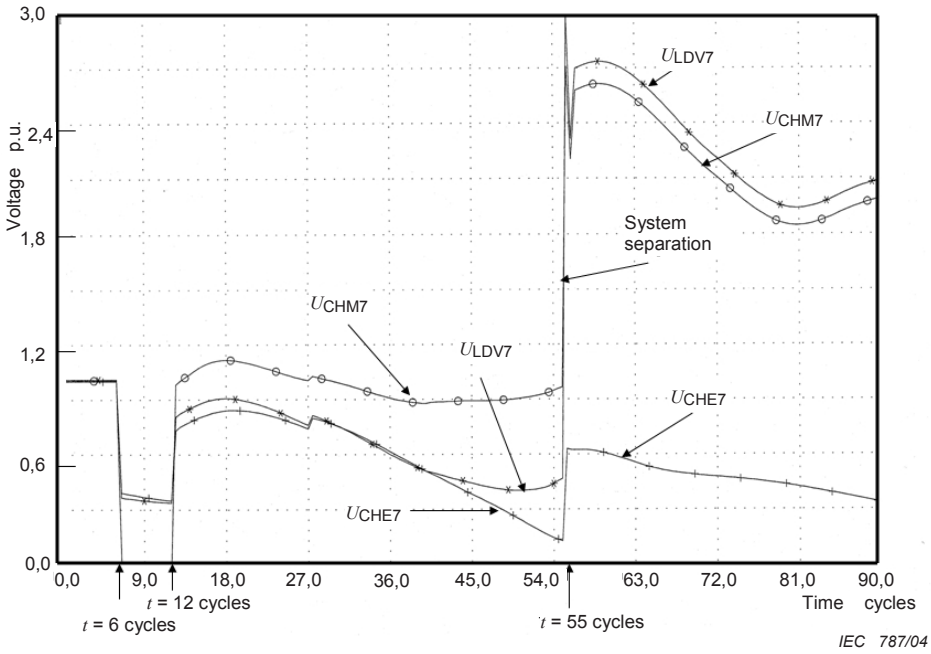

Figure 24 – TOV at CHM7, LVD7 and CHE7 from system transient stability simulation

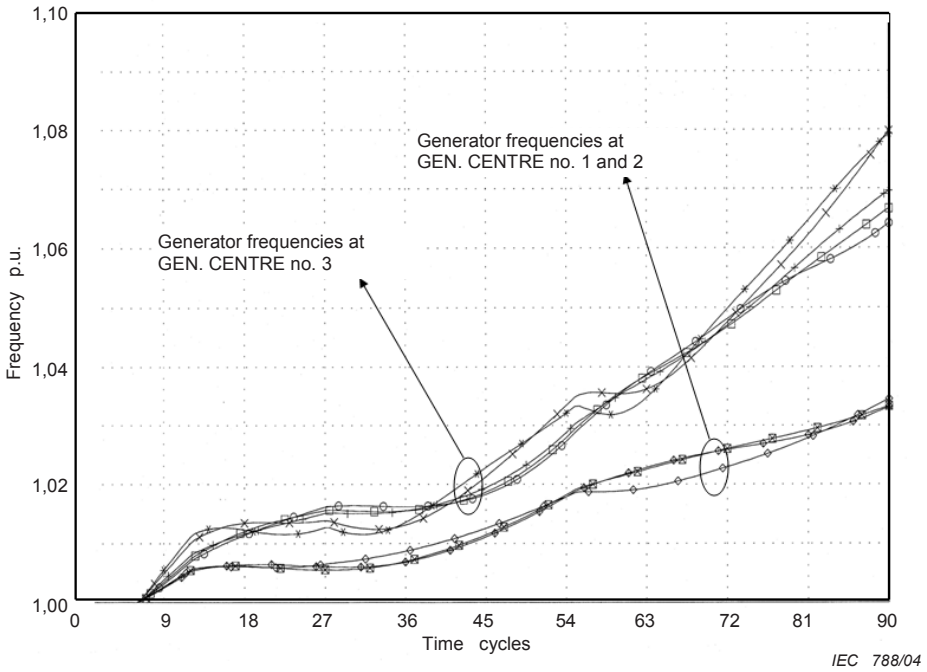

Figure 25 – Generator frequencies at generating centres Nos. 1, 2 and 3 from system transient stability simulation

12.2.3 Step 2: Electromagnetic transient simulation

12.2.3.1 System modelling

The system configuration and events leading to severe TOV that were detected in step 1 were represented by detailed three-phase electromagnetic transient simulation using the following models.

- **Dynamic sources**

In order to represent system dynamic behaviour, all generating stations and all Thévenin equivalents were simulated by the dynamic source models described in 7.4.1. The two driving signals $\delta_i(t)$ and $V_i(t)$, as illustrated in Figure 26, were calculated from the results of the stability simulation of step 1. This play-back simulation technique can only be used to include the system dynamic behaviour which was previously predicted by a stability programme. However, with the detailed representation of system non-linear characteristics such as transformer saturation and metal-oxide surge arresters, electromagnetic transient simulation will give more accurate results of TOV on the system.

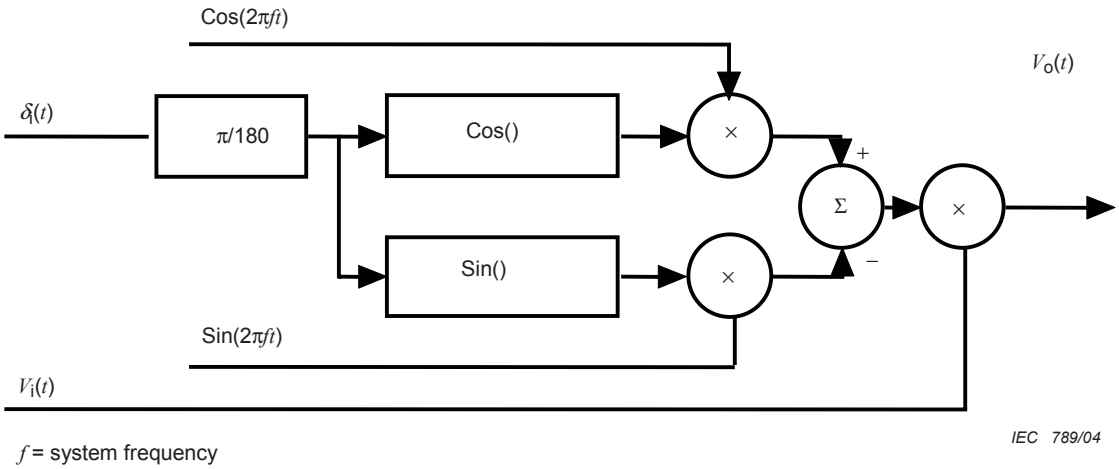

f = system frequency

$V_0(t) = V_i(t)\ \mathrm{Cos}(2\pi ft) + \delta_i(t)$, where:

$V_i(t)$ and $\delta_i(t)$ are magnitude and angle of generator internal voltage obtained from transient stability simulation

Figure 26 – Block diagram of dynamic source model [55]

- **Transmission lines**

All transmission lines were represented by three-phase distributed line models using positive and zero-sequence line parameters at fundamental frequency.

- **Transformers and auto-transformers**

Saturable transformer models have been used to represent all transformers and auto-transformers in the system. A typical saturation curve having a knee point of 1,2 p.u. and a slope of 30 % in the saturation region has been used to represent transformer saturation characteristics.

- **Loads**

All system active and reactive loads were calculated according to the system pre-fault load flow and were distributed through the sub-transmission systems which is connected to the secondary side of transformers. These loads were represented by constant impedances made up of R-L-C branches in parallel.

- **Synchronous compensators**

All synchronous compensators were represented by dynamic source models having equivalent internal impedance. All necessary data to control these dynamic sources was collected from the results of the stability simulation of step 1.

- **Static var systems (SVS) and HVDC interconnection**

All SVS and HVDC interconnection were also represented by equivalent dynamic source models. The internal impedances of these equivalent dynamic source models were set so high that they would not modify the system strength. All necessary data to control these dynamic sources are also collected from the results of the stability simulation of step 1.

- **Metal-oxide varistors protecting series-capacitor banks**

All metal-oxide varistors protecting series-capacitor banks were simulated by non-linear models representing their V-I characteristics at low-frequency injected currents (ms wave front).

- **Surge arresters**

Two types of metal-oxide surge arresters have been used in the test case system.

- **Permanent metal-oxide surge arresters having a rated voltage of 588 kV or 612 kV**

The permanent 588 kV or 612 kV surge arresters were installed at different locations in each 735 kV substation such as: shunt reactor terminals, power transformer terminals, line side of line circuit-breakers, etc. Their switching impulse protective levels are approximately 1,90-2,0 p.u.. These metal-oxide surge arresters were simulated by non-linear models representing their V-I characteristics at low-frequency injected currents (ms wave front).

- **Automatically switched metal-oxide surge arresters (SMOSA) having a rated voltage of 484 kV [39] [55]**

The SMOSA, which were applied on line terminals of ABI7, CHB7, LVD7, CHM7 and SAG7, limit the magnitude of TOV in case of system full-load rejection (or system separation) to approximatively 1,60 p.u.. Since their rated voltage is too low to be permanently connected to the system, they must therefore be automatically switched in for a short period of time (≈ 15 s) during system disturbances by local power swing detection, by remote detection of over-frequency or by open-corridor condition. These metal-oxide surge arresters were also simulated by non-linear models representing their V-I characteristics at low-frequency injected currents (ms wave front).

- **Switching sequence**

Switching sequence leading to severe TOV, as simulated in step 1, has been repeated in electromagnetic transient simulation using time-controlled switches.

12.2.3.2 Results

The results of electromagnetic transient simulations are presented in Figures 27, 28, 29 and 30.

- **Effects of permanent surge arresters**

Figures 27 and 28 show respectively TOV at LVD7 and CHM7 obtained from electromagnetic transient simulation with 588 kV and 612 kV permanent surge arresters. It can be seen that the non-linear characteristics of these system surge arresters limit TOV following the system separation to 1,9-2,0 p.u. compared to those of 2,7 p.u. from stability simulation (see Figure 24).

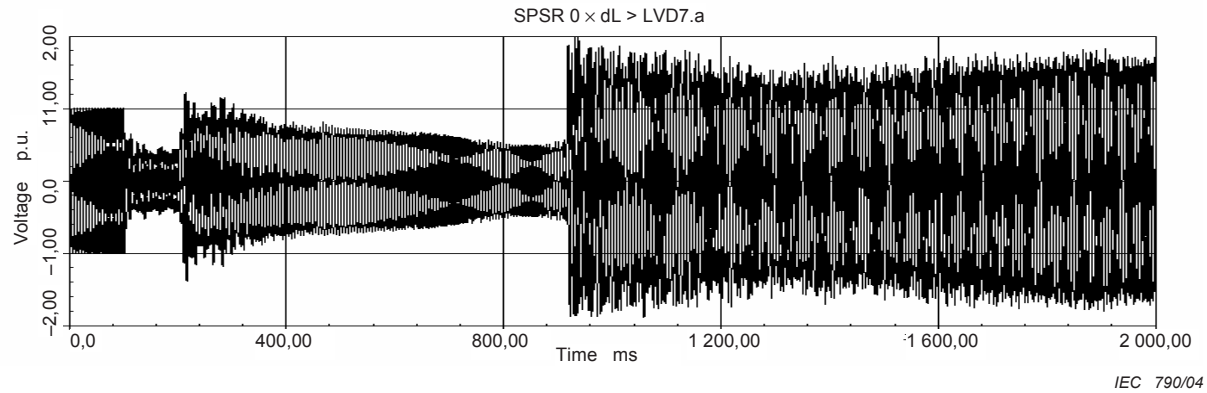

Figure 27 – TOV at LVD7 – Electromagnetic transient simulation with 588 kV and 612 kV permanent surge arresters

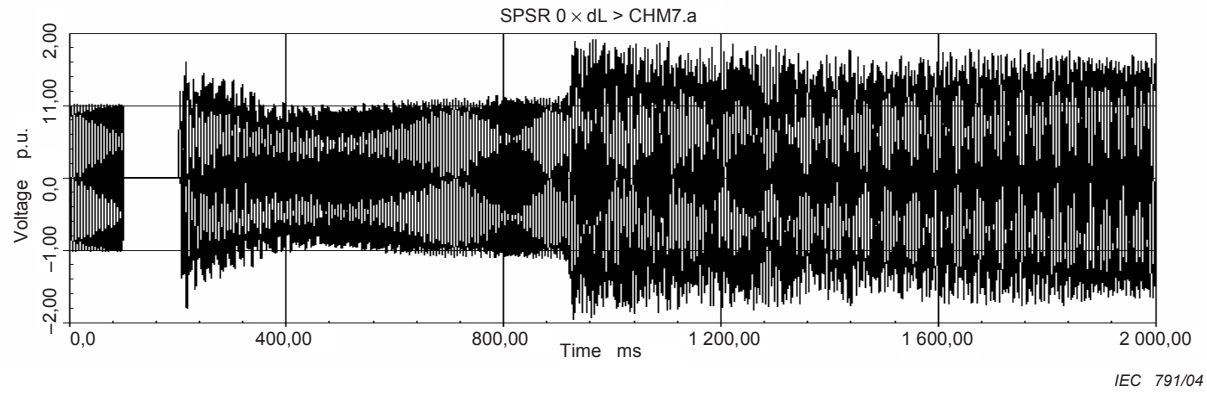

Figure 28 – TOV at CHM7 – Electromagnetic transient simulation with 588 kV and 612 kV permanent surge arresters

- **Effects of automatically switched metal-oxide surge arresters**

The results of electromagnetic transient simulation, as illustrated in Figures 29 and 30, show that TOV at LVD7 and CHM7 were further reduced to less than 1,6 p.u. with the presence of 484 kV automatically switched metal-oxide surge arresters.

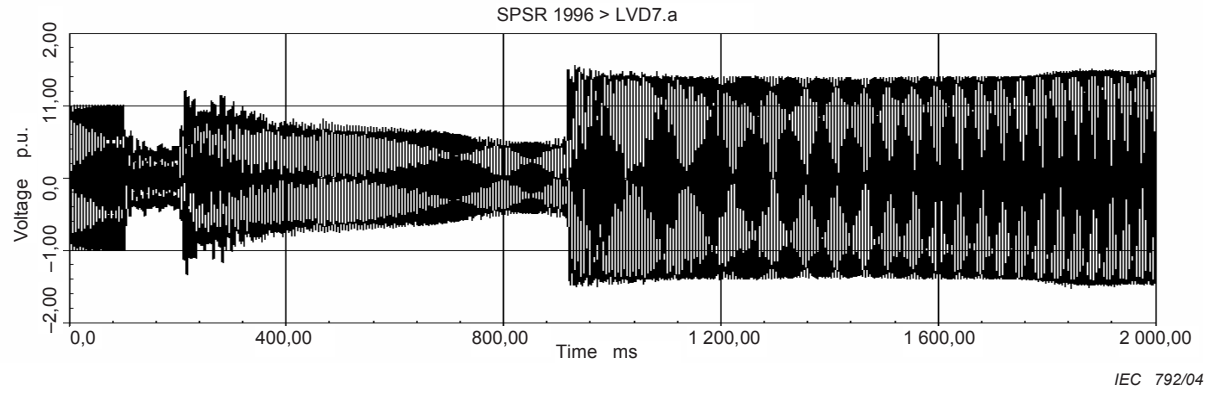

Figure 29 – TOV at LVD7 – Electromagnetic transient simulation with 484 kV switched metal-oxide surge arresters

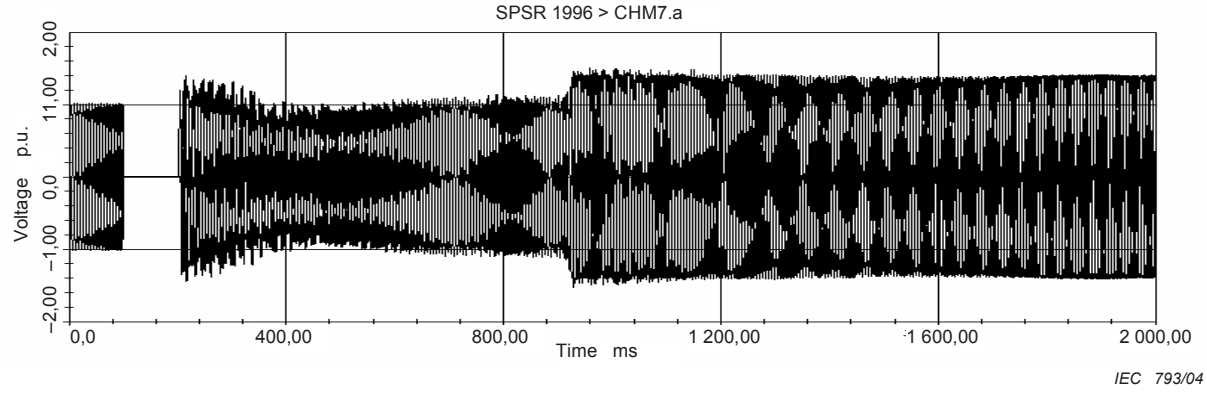

Figure 30 – TOV at CHM7 – Electromagnetic transient simulation with 484 kV switched metal-oxide surge arresters

12.2.4 Concluding remarks in terms of modelling and method

The following concluding remarks could be drawn from the results of this TOV test case:

- On a large transmission system, TOV following a full-load rejection (or a system separation) could be accurately simulated with an electromagnetic transient programme including system dynamic behaviour and system non-linear characteristics such as transformer saturation, metal-oxide surge arresters, etc.
- In order to obtain realistic TOV scenarios, all actions associated to the most relevant protections and automatic switching systems in the network should be predicted and simulated.
- In order to obtain realistic TOV results, the major part of the transmission system where disturbances take place should be represented in detail in electromagnetic transient simulation.

12.3 Case 2 (SFO) – Energization of a 500 kV line

This test case describes the study of a fictitious 500 kV line energization with the semi-statistical method (see 9.4.2). The influence of trapped charges and insertion resistors on overvoltage levels will be studied. Different configurations will be compared with help of the failure rate.

12.3.1 Input data and modelling

12.3.1.1 Diagram (Figure 31)

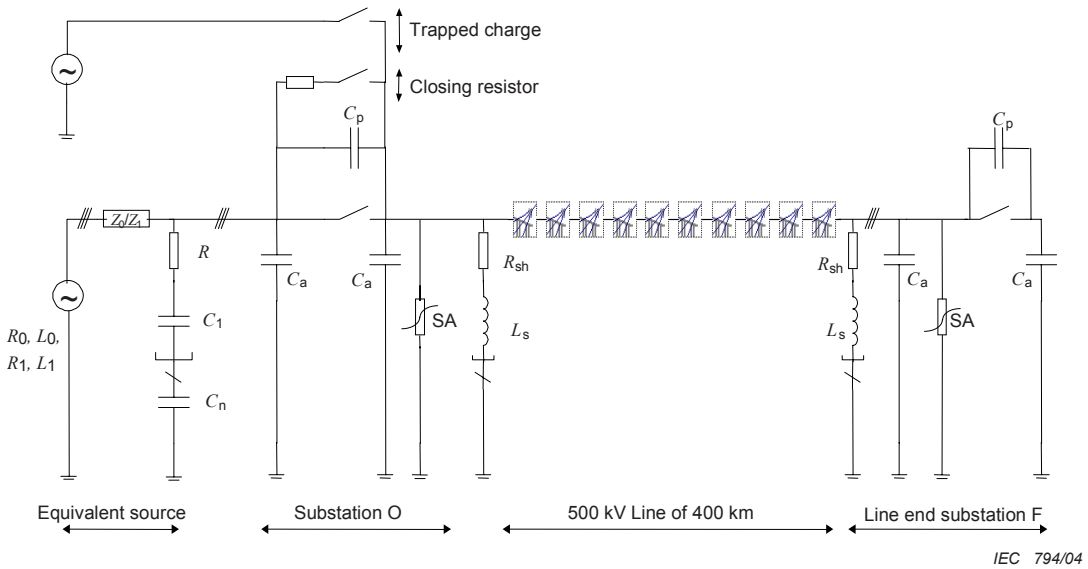

Figure 31 – Representation of the system

12.3.1.2 Short-circuit power

The source is represented by a perfect voltage source and a resonant circuit at a frequency of 1 500 Hz (see Table 14).

Table 14 – Source side parameters

U_n	Nominal voltage (V)	525 000
P_{cc3}	Three-phase short-circuit power (VA)	3,00 10^9
P_{cc1}	Single-phase short-circuit power (VA)	9,52 10^8
f	Resonance frequency (Hz)	1500
τ of the source	Time constant (s)	5,00 10^{-2}
I_{cc3}	Three-phase short-circuit current (A)	3299
I_{cc1}	Single-phase short-circuit current (A)	1047
L_1	Positive-sequence inductance (mH)	9,74
L_0	Zero-sequence inductance (mH)	72,6
R_1	Positive-sequence resistance (Ω)	0,195
R_0	Zero-sequence resistance (Ω)	1,45
C_1	Stray phase capacitance (μF)	1,15
C_n	Stray neutral capacitance (μF)	0,537
R	Damping resistance (Ω)	73,5

12.3.1.3 Substation earthing (7.5.12)

The earth impedance is represented by a 5 Ω resistance.

12.3.1.4 Surge arresters (7.5.11)

Surge arresters are modelled by their $U(I)$ characteristic. Concerning switching transient, they are characterized by their rated voltage U_r, their continuous operating voltage, U_c and their class. U_c depends on steady-state voltages that may appear in the network (see Table 15).

Table 15 – Characteristics of the surge arresters

U_r	Rated voltage (kV)	444
U_c	Continuous operating voltage (kV)	350
Cl	Class (CEI)	5
U(1kA)	Residual voltage at 1 kA (kV)	864

12.3.1.5 Shunt reactor

The compensation factor for this study is 70 %, which is a typical value for an EHV line. Fifty per cent of the inductance is connected at each end of the line (see Table 16).

Table 16 – Characteristics of the shunt reactor

C_{line}	Line capacitance (μF)	5,28
α	Compensation factor	0,7
L_s	Compensation coil inductance (H)	5,488
R_{sh}	Damping resistor (Ω)	3,45